Research Article

Nonlinear Frequency Domain Solution Method for Aerodynamic and Aeromechanical Analysis of Wind Turbines

Shine Win Naung, Mohammad Rahmati*, Hamed Farokhi
Department of Mechanical and Construction Engineering, Faculty of Engineering and Environment, Northumbria University, Newcastle upon Tyne, United Kingdom, NE1 8ST

ABSTRACT

The aerodynamic simulations of wind turbines are typically carried out using a steady inflow condition. However, the aerodynamics and aeroelasticity of wind turbine blades can be significantly affected by inflow wakes due to the environmental conditions or the presence of neighbouring wind turbines. In this paper, the effects of flow unsteadiness on the aerodynamics and aeroelasticity of the wind turbine rotor are investigated. It is found that the unsteadiness of the wake can have an impact on the aerodynamic flow field around the wind turbine rotor and it could also influence the aeroelasticity of the wind turbine. One of the distinctive features of this paper is the application of the highly efficient nonlinear frequency domain solution method for modelling harmonic disturbances for the aerodynamic and aeromechanical analysis of wind turbines. A test case wind turbine is selected for the aerodynamic and aeromechanical analysis as well as for the validation of the method used. The effects of different material properties along with a large vibration amplitude on the aeroelasticity parameter known as aerodynamic damping of the wind turbine blade are also investigated in the present work. Compared to the conventional time domain solution methods, which require prohibitively large computational cost for modelling and solving aerodynamics and aeroelasticity of wind turbines, the proposed frequency domain solution method can reduce the computational cost by one to two orders of magnitude.

Keywords
wind turbines; inflow wakes; aerodynamics; aeroelasticity; computational fluid dynamics; nonlinear frequency domain method

***Corresponding Author**
Email address: mohammad.rahmati@northumbria.ac.uk

1. INTRODUCTION

Wind turbines are affected by the dynamic loading over the entire life cycle. The sizes of the wind turbines are being increased to meet the demands of clean energy produced from renewable energy resources. Technical advances and significant efforts made over the last decade have led to offshore wind turbines with considerably longer blades to capture the wind energy more effectively and efficiently. As a result, aeroelastic instabilities such as flutter are becoming the common problems linked to the structural failures of wind turbine blades [1]. The objective of this paper is to numerically investigate the aerodynamics and aeroelasticity of the wind turbine blades taking various sources of flow unsteadiness into account using a high-fidelity computational method at an affordable computational cost.

A fluid-structure interaction (FSI) method coupling the fluid solver and the structure solver is required to solve the aeroelasticity problems. Specialist wind turbine simulation codes which employed the blade element momentum (BEM) method [2] are typically used to design and analyse the aerodynamics of most wind turbines due to the advantage of fast computation. Lin et al. [3] studied the nonlinear aeroelasticity of wind turbine blades using BEM theory and mixed-form formulation of geometrically exact beam theory (GEBT). Fernandez et al. [4] proposed a methodology for the aeroelasticity analysis of a wind turbine blade based on BEM and Finite Element (FE) models. Likewise, Rafiee et al. [5] conducted an aeroelastic analysis of a wind turbine blade coupling the BEM and FE methods. In these studies, the aerodynamic loads are obtained from the BEM models. Although the BEM models are computationally fast and efficient, they are incapable of capturing flow structures and flow details which results in a lack of understanding on the aerodynamics of wind turbines. Therefore, a high-fidelity computational model is required to capture the necessary flow details.

The vortex models employing prescribed-wake methods or free-wake methods are also used to model and analyse the wake structures and aerodynamics of wind turbines. Lee et al. [6] used an unsteady vortex-lattice method to investigate the aerodynamic performance and wake structures of a wind turbine. Riziotis et al. [7] and Jeong et al. [8] applied a free-wake model to study the aerodynamics and aeroelasticity of wind turbine blades under different conditions. Rodriguez et al. [9-10] also proposed a coupled aeroelastic free-vortex method for the aeroelasticity analysis of offshore wind turbines. The vortex models can better predict the wake and unsteady flow compared to the BEM models. However, the viscous effects are neglected by most vortex models which limits their applications for the aerodynamics and aeroelasticity of wind turbines to a certain extend. Furthermore, the vortex models are computationally more expensive than the BEM models.

Computational Fluid Dynamics (CFD) methods, either based on Reynolds Averaged Navier-Stokes (RANS) equations for steady simulations or Unsteady Reynolds Averaged Navier-Stokes (URANS) equations for unsteady simulations, are widely used in the wind energy industry to optimise the performances of wind turbines due to their capabilities of modelling steady and unsteady flows and accurately predicting flow behaviours [11-13]. CFD methods are also coupled with a structural model to study fluid-structure interactions and aeroelasticity of wind turbines. Lin et al. [14] proposed an FSI modelling method for the wind turbine blade using CFD and FE models and calculated its structural responses such as stress distribution and blade tip deflections. Likewise, Dai et al. [15] analysed the aeroelasticity of wind turbine blades under different yaw conditions using CFD and FE models. Dong et al. [16] developed a coupled CFD and Computational Structural Dynamics (CSD) method based on the URANS model to predict unsteady aerodynamic loads on the wind turbine blade and its time-varying aeroelastic responses. Similarly, Dose et al. [17-18] employed a coupled CFD-CSD model to perform FSI simulations of wind turbines. The main disadvantage of the CFD methods is their large computational resources requirement [19-20]. Significant computational resources and long runtimes are typically required by the URANS computations.

Based on the above literature review, it is clear that the computational cost of high-fidelity aerodynamic and aeroelasticity simulations remains the main challenge for the industry not only for wind turbines but also for other turbomachines. Numerous studies have been conducted over the last decade with the purpose of developing efficient numerical methods which can reduce the computational cost. A time-linearized harmonic frequency-domain method is one of the outcomes and it was widely used in the turbomachinery industry [21-22]. This method was later replaced by the harmonic balance method of Hall et al. [23], the phase solution method of He [24], and Rahmati et al. [25-26] for modelling harmonic disturbances and flow nonlinearities. Rahmati et al. [27] developed a nonlinear frequency domain solution method for the aeroelasticity analysis of multiple blade row configurations. It is found that a fully coupled multiple blade row model yields better accuracy in predicting flutter behaviour of the turbomachines than the simplified isolated one [28]. Although frequency domain methods are typically used for the aeromechanical analysis of turbomachinery applications, only a few studies recently applied these methods to wind turbine applications [29-34]. This has motivated the authors to seek an efficient numerical method employing a frequency domain method for the aerodynamic and aeroelasticity simulations of wind turbines at an affordable computational cost without compromising accuracy in predicting unsteady flows. Therefore, the nonlinear frequency domain solution method, developed by Rahmati et al. [27-28], which has been validated and revealed that this method can not only predict aerodynamics and aeroelasticity of multi-stage turbomachines accurately but also reduce the computation time significantly, is extended in this paper to be applied to the aerodynamic and aeromechanical simulations of wind turbines.

The MEXICO (Model Rotor Experiments In Controlled Conditions) Experiment wind turbine [35-38], is selected to be studied in the present work. First, the aerodynamic analysis of this wind turbine is conducted by generating inflow wakes and analysing their effects on the unsteady flow field. The aeromechanical analysis of this wind turbine is then performed. The frequency domain solution method is used in this study and it is validated against the conventional time domain solution method.

This paper is structured as follows: Section (2) describes the selected MEXICO-Experiment wind turbine. The numerical methodology which includes the employed computational method, the computational domain and grid for the CFD simulations and the generation of the inflow wakes are explained in section (3). The numerical results are discussed in section (4) and the key findings are summarised in the conclusions section.

2. THE MEXICO-EXPERIMENT WIND TURBINE

The MEXICO Experiment is a wind tunnel experiment that was performed in the German-Dutch Wind Tunnel (DNW) [35-38]. The blade is 2.04 m long and the rotor diameter is 45 m. Numerical simulations have also been conducted previously on this wind turbine [39-43]. The wind speed and the rotational speed selected in this study are 15 m/s and 424.5 RPM, respectively, and the blade pitch angle is -2.3 degrees. The proposed nonlinear frequency domain solution method is employed for both aerodynamic and aeromechanical analysis of this wind turbine. Due to the lack of experimental data or previous studies for the types of analysis discussed in this paper, the conventional time domain solution method is used for validation purposes. For the aeromechanical analysis, the modal analysis is conducted before the flow simulation and the natural frequencies and the structural mode shapes are extracted from the modal analysis. To investigate the effect of material properties on the aeroelasticity of the blade. two different materials are considered and used in this study. The first one is an Aluminium Alloy with a density of 2770 kg/m^3, a Young's modulus of 7.1E+10 Pa, and a Poisson ratio of 0.27 to be similar to the one used in the experiment. The other one is a composite material, approximated by the orthotropic material properties as presented in Table. 1, as modern wind turbines are designed using composite materials which can reduce weight. It should be noted that the main purpose of this analysis is to investigate the effect of material properties on the aeroelasticity parameter, especially aerodynamic damping, of the blade. The material properties used in this paper are approximations and may not necessarily represent the actual properties used for commercial wind turbine blades.

Table 1. Orthotropic material properties of the composite material used in the paper

Density (kg/m^3)	1550
Young's Modulus-X (Pa)	1.1375E+11
Young's Modulus-Y (Pa)	7.583E+09
Young's Modulus-Z (Pa)	7.583E+09
Poisson's Ratio-XY	0.32
Poisson's Ratio-YZ	0.37
Poisson's Ratio-XZ	0.35
Shear Modulus-XY (Pa)	5.446E+09
Shear Modulus-YZ (Pa)	2.964E+09
Shear Modulus-XZ (Pa)	2.964E+09

3. NUMERICAL METHODOLOGY

3.1 Computational Method

In this paper, the CFD method is used for aerodynamic computation. For the modelling and simulation of the FSI problem, the modal coupling method is employed. With this method, the modal analysis needs to be conducted prior to the flow simulation to calculate the natural frequencies and the mode shapes of the blade structure. These information are then imported into the flow simulation to define the blade vibration in the CFD analysis. The modelling and computation of the unsteady flow due to fluid-structure interactions are all performed in the CFD environment. The details of the employed numerical method are described below.

3.1.1 Flow Governing Equations

The aerodynamic simulation is performed by a three-dimensional, density-based, structured, and multi-block finite volume CFD method. The flow is governed by Navier-Stokes equations and the general Navier-Stokes equations written in a Cartesian frame can be expressed as:

$$\frac{\partial}{\partial t}\int_{\Omega} U d\Omega + \int_{S} \vec{F}_I \,.\, d\vec{S} + \int_{S} \vec{F}_V \,.\, d\vec{S} = \int_{\Omega} S_T d\Omega \qquad (1)$$

where Ω is the volume, S is the surface, U is the vector of the conservative variables, S_T is the source term, and $\vec{F}_I$and $\vec{F}_V$are the inviscid and viscous flux vectors, respectively. URANS model is employed in this study and the standard Spalart-Allmaras model is used for the turbulence model. The above equation can be simply expressed in a semi-discrete form as [25-28]:

$$\frac{\partial}{\partial t}(U) = R(U) \qquad (2)$$

where R is the lumped residual and the source term. Traditionally, the Navier-Stokes equations are solved in a CFD solver at every time-step in the time domain. This method is referred to as the time domain method in this paper.

3.1.2 Frequency Domain Solution Method

In wind turbine aerodynamics and aeroelasticity, the unsteadiness of the flow can be associated with the inflow wake or the blade deflection, which are periodic in time. With the frequency domain solution method, the conservative flow variables from the Navier-Stokes equations can be decomposed into the time-averaged and the unsteady fluctuations. Therefore, the unsteady conservative flow variables subject to the source of flow unsteadiness can be represented by the Fourier series for a prescribed fundamental frequency, ω, which can be related to the inflow wake frequency or the blade vibration frequency, and the specified number of harmonics, m, as expressed in Eq. (3).

$$U = \bar{U} + \sum_{m=1}^{M}[A_U \sin(m\omega t) + B_U \cos(m\omega t)] \tag{3}$$

where $\bar{U}$, A_U, and B_U are the Fourier coefficients of the conservation variables. The number of harmonics or the order of Fourier series is an input of the applied numerical method, and the accuracy and resolution of the unsteady flow solution can be controlled through the order of Fourier series. Substituting this Fourier decomposition (i.e. Eq. (3)) into the Navier-Stokes equation (i.e. Eq. (2)) yields a new set of unsteady Navier-Stokes equations in the frequency domain as follow:

$$\omega \sum_{m=1}^{M}[mA_U \cos(m\omega t) - mB_U \sin(m\omega t)] = R \tag{4}$$

With the frequency domain solution method, these new set of Navier-Stokes equations are solved in the frequency domain. The unsteady period is equally divided into $N = (2m+1)$ time levels and the system of nonlinear equations coupling all N time levels are solved iteratively.

As the sources of flow unsteadiness discussed in this paper are based on a periodic inflow or periodic blade displacement, the fundamental mode (one harmonic) is considered enough and therefore, Eq. (3) and Eq. (4) are re-written using one harmonic as:

$$U = \bar{U} + [\, A_U \sin(\omega t) + B_U \cos(\omega t)] \tag{5}$$

$$\omega[A_U \cos(\omega t) - B_U \sin(\omega t)] = R \tag{6}$$

At three distinctive temporal phases, Eq. (5) can be written as follows:

$$U_0 = \bar{U} + B_U \qquad \omega t = 0 \tag{7.a}$$
$$U_{\pi/2} = \bar{U} + A_U \qquad \omega t = \pi/2 \tag{7.b}$$
$$U_{-\pi/2} = \bar{U} - A_U \qquad \omega t = -\pi/2 \tag{7.c}$$

The three Fourier coefficients - $\bar{U}$, A_U, and B_U – can be calculated based on the above three equations. Substituting these coefficients into Eq. (6) at the three phases yields the following equations:

$$\omega\left(\frac{U_{\pi/2} - U_{-\pi/2}}{2}\right) - R_0 = 0 \tag{8.a}$$
$$\omega\left(U_0 - \frac{U_{\pi/2} + U_{-\pi/2}}{2}\right) + R_{\pi/2} = 0 \tag{8.b}$$
$$\omega\left(U_0 - \frac{U_{\pi/2} + U_{-\pi/2}}{2}\right) - R_{-\pi/2} = 0 \tag{8.c}$$

These new sets of Navier-Stokes equations are simultaneously solved by a CFD solver in a similar way to that of the steady-state equations with the extra term being treated as a source term [25-28], thereby saving the computation time significantly compared to the conventional time domain method. A central scheme is used for the spatial discretization which is based on a cell centred control volume approach and a four-stage Runge–Kutta scheme is used for the temporal discretization. The flow solution obtained from the frequency domain solution method can be reconstructed in time to have the unsteady periodic flow in time history.

This method belongs to a family of frequency domain methods such as the harmonic balance method of Hall et al. [23] and the phase solution method of He [24]. Moreover, the proposed nonlinear frequency domain solution method is initially developed by Rahmati et al. [25-28] for the aeromechanical analysis of multi-stage turbomachines and this method is now extended to be applied to wind turbines. The readers are referred to the aforementioned studies for the fundamental formulation and implementation of the frequency domain methods.

3.1.3 Fluid-Structure Interaction

The modal coupling method is employed in this paper in order to integrate the blade vibration in the flow simulation to perform the aeromechanical simulation of the wind turbine. The modal analysis using a structure solver is required before conducting the flow simulation to calculate the natural frequencies and the mode shapes of the structure.

The solid mechanics of a structure is governed by the following equation:

$$[M]\frac{\partial^2 \vec{d}}{\partial t^2} + [C]\frac{\partial \vec{d}}{\partial t} + [K]\vec{d} = \vec{f} \tag{9}$$

where $[M]$ is the mass matrix, $[C]$ is the damping matrix, $[K]$ is the stiffness matrix, $\vec{d}$ is the displacement of the structure, and $\vec{f}$ is the external load.

The global displacement of the structure can be written as:

$$\vec{d} = \sum_{i=1}^{n_{modes}} q_i \vec{\phi}_i \tag{10}$$

where q_i is the generalised displacement and $\vec{\phi}_i$ is the mode shapes of the structure normalised by the mass.

Eq. (10) can be written in matrix form as:

$$\vec{d} = [\phi]\vec{q} \tag{11}$$

Substituting Eq. (11) into Eq. (9) and multiplying with $[\phi]^T$ yields the following equation.

$$[\phi]^T[M][\phi]\frac{\partial^2 \vec{q}}{\partial t^2} + [\phi]^T[C][\phi]\frac{\partial \vec{q}}{\partial t} + [\phi]^T[K][\phi]\vec{q} = [\phi]^T\vec{f} \tag{12}$$

Using mass-normalised mode shapes should satisfy that the generalised mass matrix is the unit matrix (i.e. $[\phi]^T[M][\phi] = [I]$) and the generalised stiffness matrix is a diagonal matrix in which the elements are the square of the mode frequency (i.e. $[\phi]^T[K][\phi] = diag[{\omega_i}^2]$). Furthermore, assuming a Rayleigh damping, the generalised damping matrix can be expressed as: $[\phi]^T[C][\phi] = diag[2\xi_i\omega_i]$, where ω_i is the natural frequencies of the structure and ξ_i is the damping coefficient [44,45].

Substituting them into Eq. (12) and expressing the system for every mode *i* yields the following equation:

$$\frac{d^2q_i}{dt^2} + 2\xi_i\omega_i\frac{dq_i}{dt} + \omega_i^2 q_i = \vec{\phi}_i^{\,T}\vec{f} \tag{13}$$

Prior to the flow simulation, the modal analysis needs to be performed first. A structure code using a Finite Element Analysis (FEA) method is used for the modal analysis to compute the natural frequencies and the mode shapes of the structure. Then, these information are imported into the flow simulation for the blade vibration.

The generalised displacement q_i must be specified for the considered amplitude of deformation and it can be written as:

$$q_i(t) = \bar{q} + q_A\cos(\omega_i t) \tag{14}$$

where $\bar{q}$ and q_A are the mean value and amplitude of the displacement, respectively. Having this information, the flow solver computes the deformation of the structure by solving Eq. (10) and solves the Navier-Stokes equations using the deformed blade.

The flow chart of the employed FSI computation is presented in Fig. 1. Steady simulation is first performed, and the steady solution is defined to be the initial condition in the unsteady simulation. Before conducting the unsteady simulation, the natural frequencies and the mode shapes of the blade structure, obtained from the modal analysis in an FEA environment, need to be imported into the flow solver. Afterwards, together with the specified time-averaged and amplitude of the generalised displacement, the flow solver computes the generalised displacement q using Eq. (14). Based on the generalised displacement, the flow solver then computes the total deformation of the blade structure and deforms the mesh. Using the deformed blade, the CFD analysis is performed by solving the Navier-Stokes equations. In the case of the time domain solution, these steps are performed at every time step until the flow solution reaches steady and periodic condition. On the other hand, with the frequency domain solution, the unsteady period is equally divided into $N = (2m+1)$ time levels and the system of nonlinear equations coupling all N time levels are solved iteratively in a similar way to that of the steady-state equations with the extra term being treated as a source term. The frequency domain solution can also be reconstructed in time to have the flow solution in time history. Unsteady flow characteristics are calculated and produced from the analysis. Pressure distributions on the blade surfaces are particularly calculated which is used to calculate the forces and aerodynamic power acting on the blade structure.

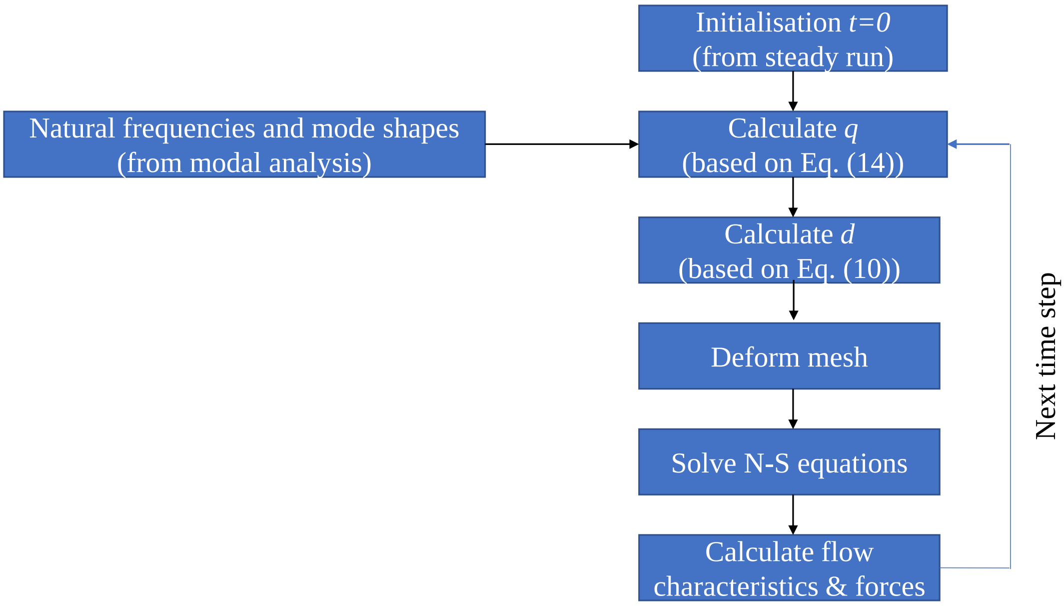

(a)

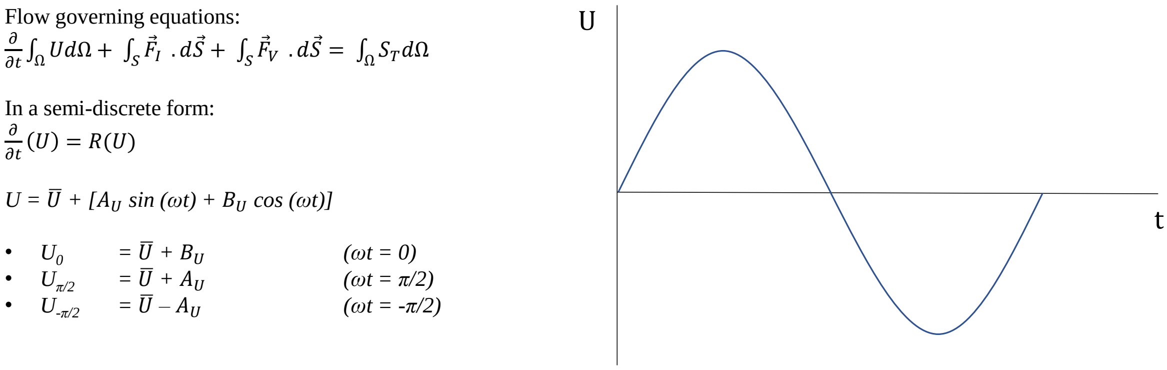

(b)

Figure 1. (a) Flow chart of the modal coupling FSI method and (b) the flow solution of the frequency domain solution method using one harmonic

3.1.4 Boundary Conditions

The solid wall boundary condition is applied to the blade and the hub. Stationary wall boundary is defined in the aerodynamic analysis whereas the deforming wall boundary with a periodic displacement is defined in the aeromechanical analysis. In the case of the aeromechanical simulation, the global displacement of the blade structure is obtained using Eq. (10) based on the specified generalised displacement and the imported natural frequency and the mode shape. Hence, the global displacement of the blade becomes:

$$d(t) = \bar{d} + d_A \cos(\omega_i t) \tag{15}$$

where $\bar{d}$ and d_A are the mean value and amplitude of the blade displacement, and the blade wall boundary is deformed with respect to the blade displacement.

The external boundary condition, which is a non-periodic one, is defined to treat the far-field boundaries dealing with the external flow computations. A full rotor model with all three blades without using periodic boundaries is used for the time domain method. On the other hand, a single passage domain is used for the frequency domain solution method, and the harmonic components are phase-shifted between the periodic boundaries by a given Inter Blade Phase Angle (IBPA), σ, as expressed in the following equations [25-28] where the subscript 1 and 2 are corresponding to the referenced passage and its neighbouring one, respectively.

$$A_{U,2} = A_{U,1}\cos(\sigma) - B_{U,1}\sin(\sigma) \tag{16.a}$$

$$B_{U,2} = A_{U,1}\sin(\sigma) + B_{U,1}\cos(\sigma) \tag{16.b}$$

3.2 Computational Domain and Grid

The three-dimensional computational domain and grid are created using a Rounded Azimuthal O4H topology in a structured grid generator. The grid consists of five blocks. An O-mesh is used in the skin block surrounding the blade whereas an H-mesh is used in other blocks such as the inlet block, the outlet block, the upper block above the blade section and the lower block under the blade section. The first layer's thickness is 1e-5 meters to keep the y^+ value less than one. The flow inlet and outlet are located 10R upstream of the rotor and 25R downstream of the rotor, respectively, and the far-field boundary is placed 5R from the origin of coordinates where R is the rotor radius. There are 4.5 million grid points in a single passage domain which is 1/3 of the full rotor. The computational domain of a single passage, the mesh around the blade in the blade-to-blade view and the 3D view of the mesh of the blade are shown in Fig. 2. A single passage domain (i.e. 120 degrees grid) is used for the frequency domain method whereas a full passage domain (i.e. 360 degrees grid including all three blades) is used for the time domain method.

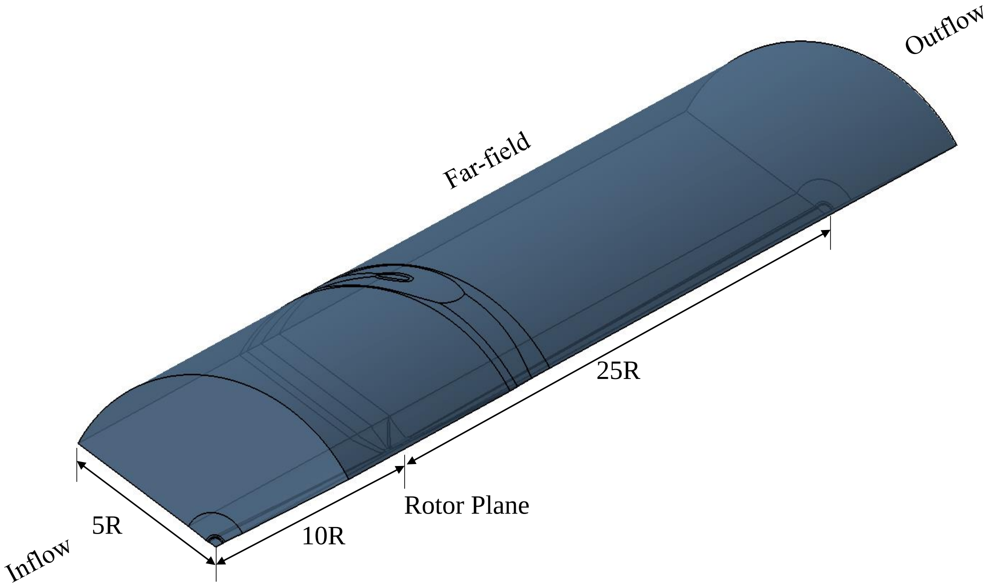

(a)

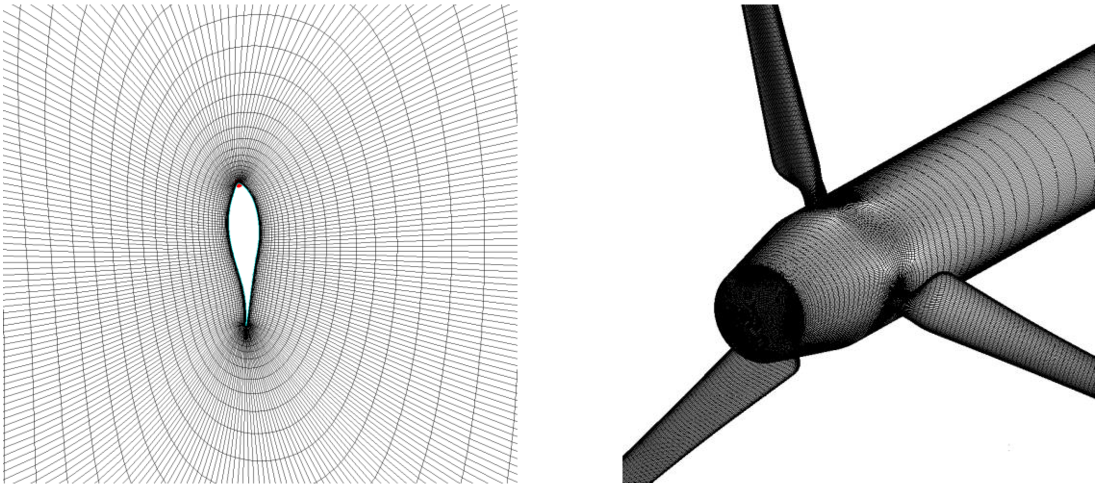
(b) (c)

Figure 2. (a) Computational domain, (b) grid in blade-to-blade view and (c) 3D view of the MEXICO-Experiment wind turbine rotor

3.3 Inflow Wake Generation

The majority of the previous studies considered a steady wind flow for the simulations, while in reality, the nature of the wind is not steady. The wind speed changes in time or is affected by the objects present in the surroundings such as nearby wind turbines. The flow unsteadiness can impose a significant impact on wind turbine aerodynamics or aeroelasticity. In order to consider the unsteady nature of inflow, a wake is introduced at the inlet to study its effects on the aerodynamics of the wind turbine rotor. In this study, a harmonic wake is considered to represent the unsteady nature of the wind of which the speed varies in time. The inflow wind speed, w, is generated based on Fourier series as follow.

$$w = \bar{w} + w_A \sin(\omega_w t) \qquad (17)$$

where $\bar{w}$ is the averaged wind speed, w_A is the amplitude of the unsteady fluctuation, and ω_w is the frequency of the wake. For the purpose of simplicity and validation of the proposed method, only one harmonic is used to implement the harmonic inflow wakes in this study. The number of harmonics can be further increased to better represent the actual wind condition. In this analysis, the averaged wind speed is the same as the steady simulation which is 15 m/s and the amplitude of 5 m/s is selected to cover a wide range of wind speeds as well as to investigate the effect of relatively high fluctuation. Four frequencies, 5 Hz, 10 Hz, 15 Hz and 20 Hz, are considered for the wake frequencies in this work, and the effects of each frequency on the aerodynamics of the wind turbine rotor are investigated. These frequencies are particularly chosen to simulate the effects of a range of frequencies on the wind turbine rotor aerodynamics. The nonlinear frequency domain method is used for this analysis, and the results are validated against the time domain method. This marks one of the distinctive features of this paper as the majority of studies available in the literature are based on a steady inflow, and this is also the first time that the nonlinear frequency domain method is used to analyse the aerodynamics of a wind turbine based on the inflow wake.

4. RESULTS

4.1 Aerodynamic Analysis of the MEXICO-Experiment Wind Turbine

The steady pressure coefficient distributions using a steady inflow are first compared against the experiment as well as the previous simulation performed by Sorensen et al. [40] to validate the CFD model used. Figure 3 shows the comparison of the steady pressure coefficients at 25%, 35%, 60%, 82% and 92% span blade sections. As seen, slight differences are seen between the CFD simulations and the experiment at the blade inner sections, 25% and 35% blade span, due to instability in the pressure transducers which occurred during the experiment as discussed in previous studies [39-40]. Overall, the present simulation results are very close to those of Sorensen et al. [40] and they are in a good agreement with the experiment.

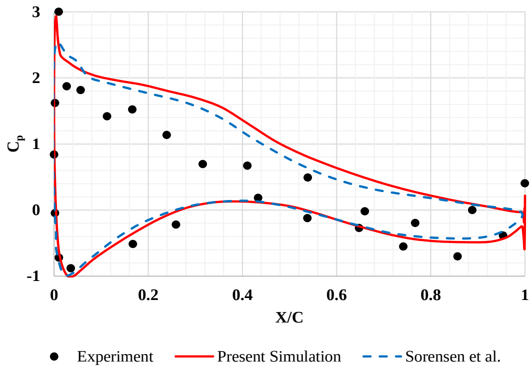

(a)

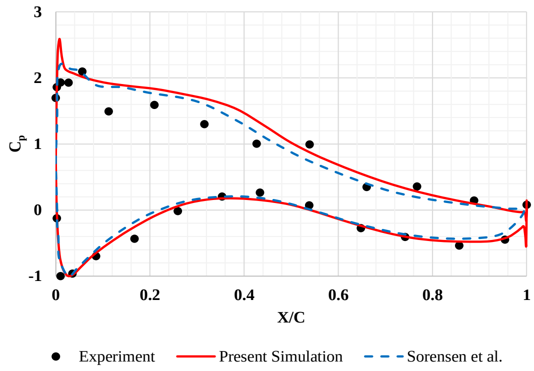

(b)

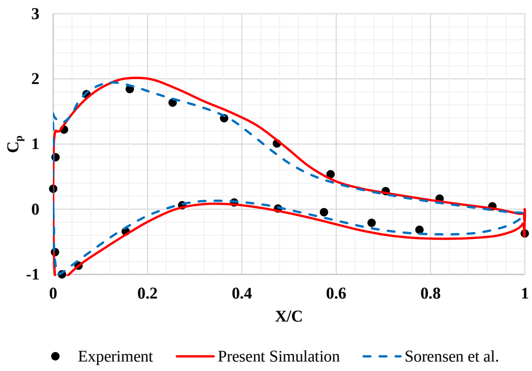

(c)

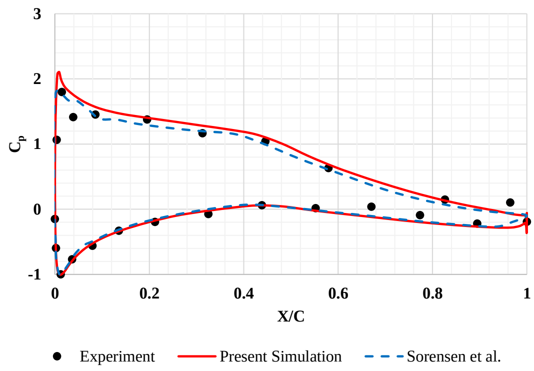

(d)

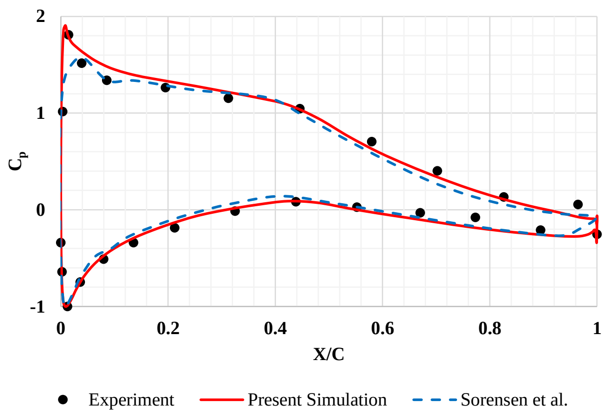

(e)

Figure 3. Pressure coefficients at (a) 25%, (b) 35%, (c) 60%, (d) 82%, and (e) 92% of the blade span obtained from the experiment *(symbol)*, the simulation performed by Sorensen et al. [40] *(dotted line)*, and the present simulation *(line)*

After having validated the CFD model used, a series of further simulations are conducted generating inflow wakes at different frequencies at the inlet. Unsteady pressure distribution can be divided into time-averaged value and amplitude of fluctuation as shown in Eq. (5), and it can be written as:

$$P = \bar{P} + P_A \sin(\omega t) + P_B \cos(\omega t) \qquad (18)$$

where $\bar{P}$ is the time-averaged pressure, and P_A and P_B are Fourier coefficients. The unsteady pressure amplitude can be defined as $\sqrt{{P_A}^2 + {P_B}^2}$.

The unsteady pressure terms are only visible in the harmonic inflow cases as the harmonic disturbances are present due to the wake. Figures 4-7 present the comparisons of the time-averaged pressure coefficient and the unsteady pressure amplitude coefficient distributions at the blade mid-span section for each frequency computed from both time domain and frequency domain methods. As seen, they are in a very good agreement in both perspectives. It is also noticed that the unsteady pressure distributions vary with different inflow wake frequencies which indicates that the flow unsteadiness due to the wake depends on the frequency. No difference is seen between different frequencies in terms of the time-averaged pressure coefficients. This is expected as the same average wind speed is used and hence the mean value of pressure distributions could be similar to each other. This behaviour is also seen at the other blade sections, but they are not shown in this paper to keep this section more concise. Good agreements between the two methods are also observed at the other blade sections.

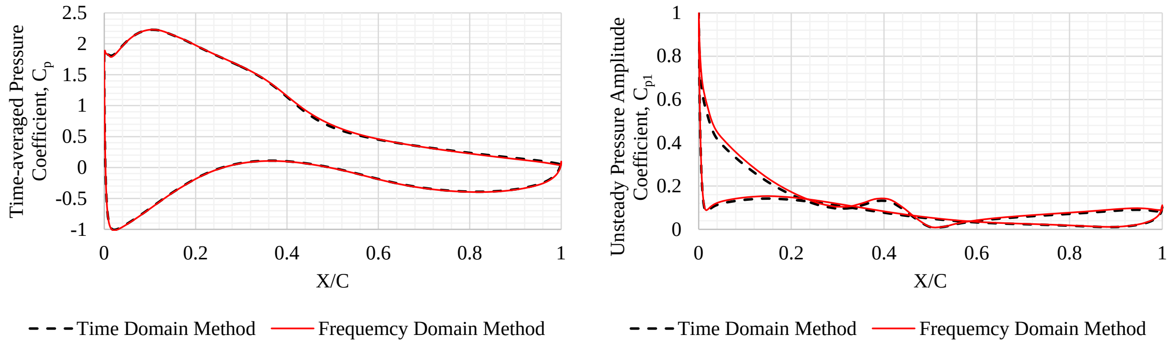

(a) (b)

Figure 4. (a) Time-averaged pressure and (b) unsteady pressure amplitude coefficients at the blade mid-span section computed from the time domain method *(dotted line)* and the frequency domain method *(line)* at the inflow wake frequency of 5 Hz

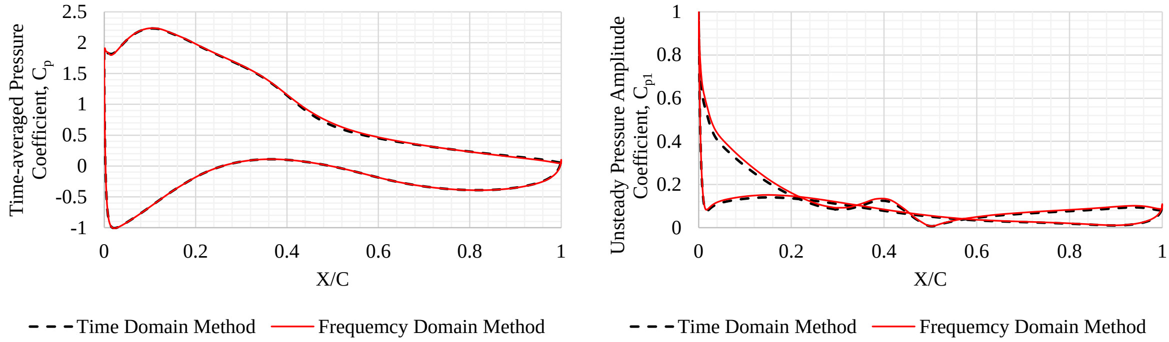

(a) (b)

Figure 5. (a) Time-averaged pressure and (b) unsteady pressure amplitude coefficients at the blade mid-span section computed from the time domain method *(dotted line)* and the frequency domain method *(line)* at the inflow wake frequency of 10 Hz

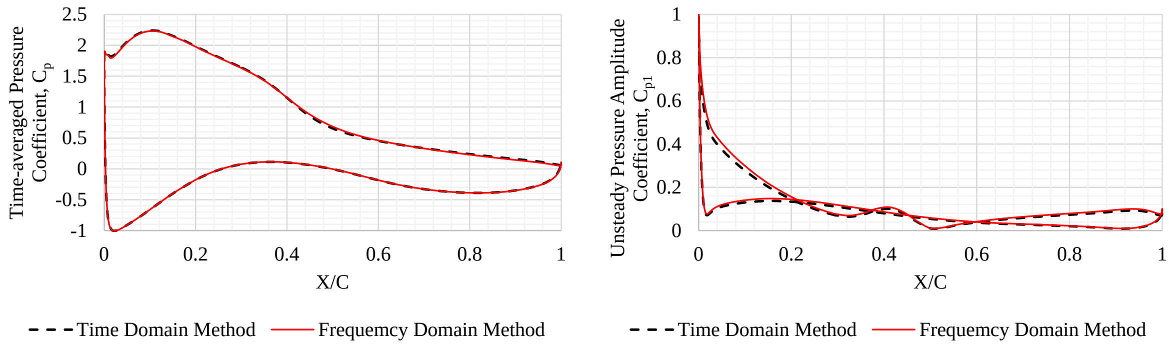

(a) (b)

Figure 6. (a) Time-averaged pressure and (b) unsteady pressure amplitude coefficients at the blade mid-span section computed from the time domain method *(dotted line)* and the frequency domain method *(line)* at the inflow wake frequency of 15 Hz

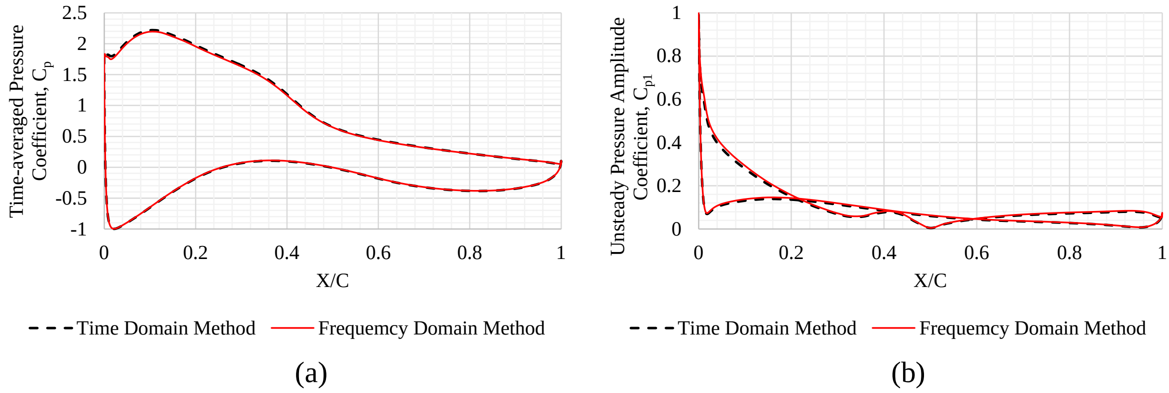

Figure 7. (a) Time-averaged pressure and (b) unsteady pressure amplitude coefficients at the blade mid-span section computed from the time domain method *(dotted line)* and the frequency domain method *(line)* at the inflow wake frequency of 20 Hz

It is now evident that the frequency domain method can be used for the computation of unsteady pressure distribution on the blade surfaces subject to the inflow wakes. However, it is also important to analyse the pressure field around the rotor. The pressure coefficient profiles along the rotation axis from one rotor diameter upstream to one rotor diameter downstream at different frequencies computed from both methods are compared in Fig. 8. As shown, the results calculated from both methods agree well with each other. Therefore, it is concluded that the unsteady pressure distribution and the flow field around the wind turbine rotor can be reliably computed using the frequency domain method.

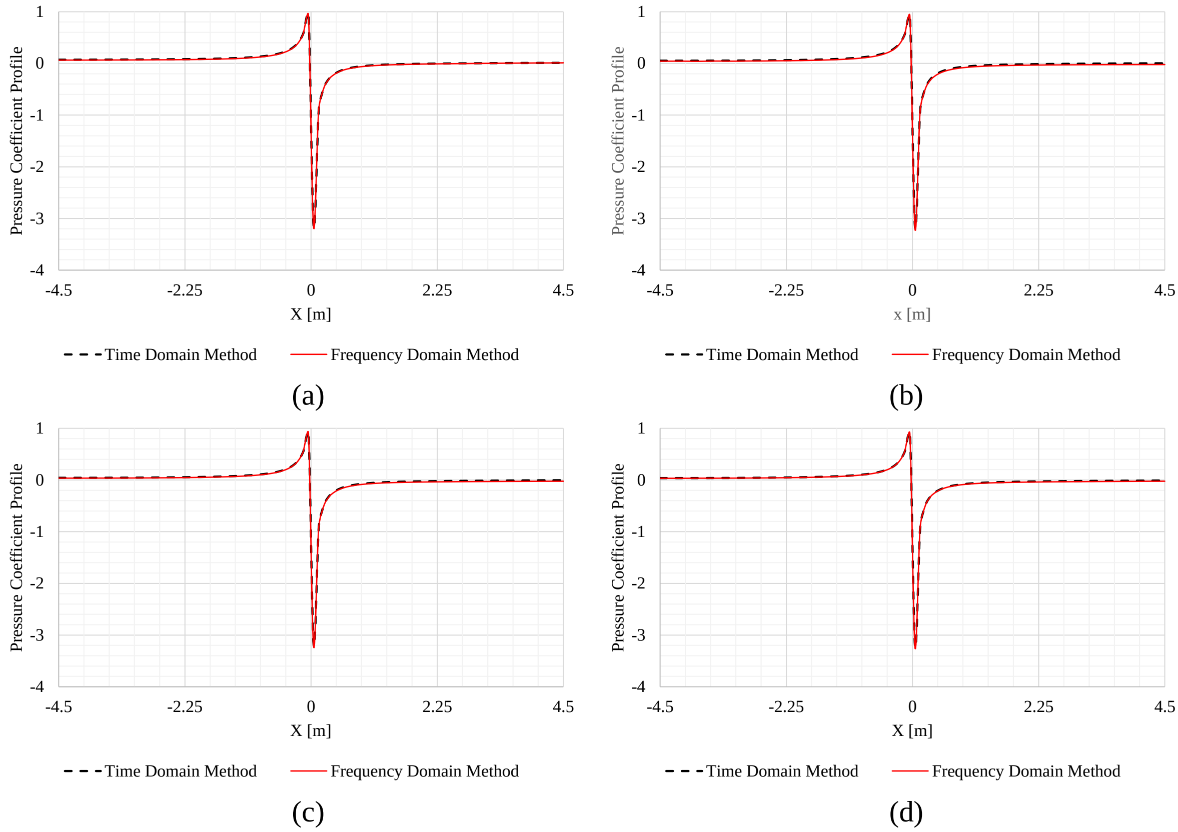

Figure 8. Pressure coefficient profiles at the wake frequencies of (a) 5 Hz, (b) 10 Hz, (c) 15 Hz, and (d) 20 Hz computed from the time domain method *(dotted line)* and the frequency domain method *(line) ('0' marks the rotor plane; negative axis and positive axis represent upstream and downstream of the rotor, respectively)*

The effect of unsteadiness of the inflow wakes on the flow field around the rotor can be identified using the velocity magnitude contours in the meridional view as well as the blade-to-blade view. Figure 9 demonstrates the instantaneous velocity fields around the wind turbine rotor in the meridional view for the steady inflow case as well as the harmonic inflow cases. It is seen that the presence of inflow wakes affects the flow around the rotor and influences the vortex shedding process. The velocity fields behind the rotor are distorted by the inflow wakes whereas the flow field is steady in the steady inflow case. The flow unsteadiness is higher at lower frequencies which is also consistent with the unsteady pressure distributions seen in Figs. 4-7. The vortex generation process is also influenced by the wakes as the velocity bubbles generated from the tip of the blade and the flow left from the blade and the hub differ with inflow wake frequencies. The flow unsteadiness and the effects of the wakes are visible at all frequencies; however, the velocity field behind the rotor is lower at 20 Hz compared to other frequencies.

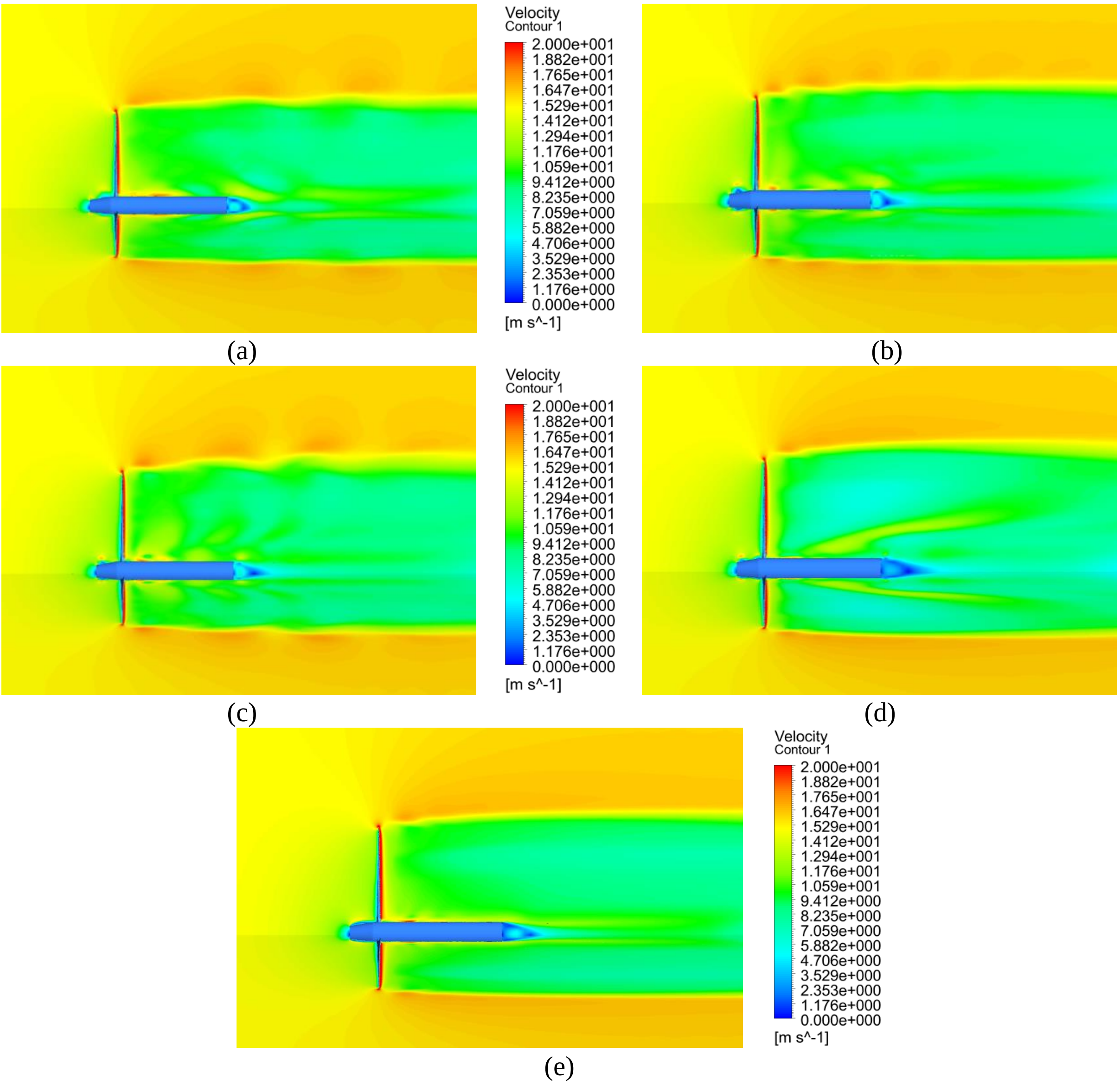

Figure 9. Velocity fields in the meridional view from (a) the harmonic inflow case at frequency = 5 Hz, (b) the harmonic inflow case at frequency = 10 Hz, (c) the harmonic inflow case at frequency = 15 Hz, (d) the harmonic inflow case at frequency = 20 Hz, and (e) the steady inflow case

Figures 10 and 11 show velocity distributions around the blade aerofoil at different wind speeds at the 25% span and 75% span, respectively, to investigate the effect of wind speed fluctuations on the flow. These two blade sections are chosen to represent the blade inner region, where it has a larger blade section pitch angle and the outer region with a lower blade pitch angle. In the blade inner region, flow separation from the suction surface of the blade is observed at higher wind speeds. However, the flow is mostly attached with a little separation near the blade trailing edge at lower wind speeds. Likewise, the separation is also larger at higher wind speeds in the blade outer region. The high-velocity concentration is found near the leading and trailing edges. Compared to the blade inner region, the velocity magnitude is higher in the outer region.

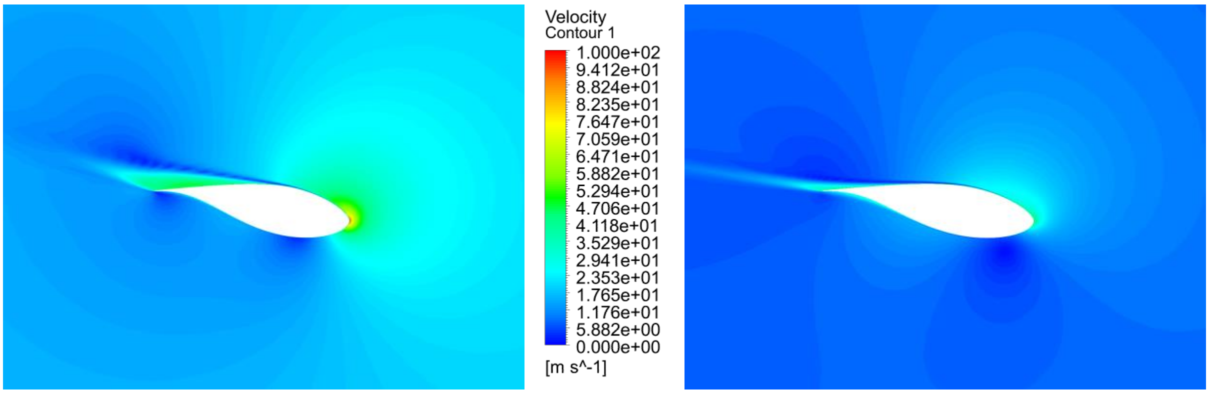

(a) (b)

Figure 10. Velocity distributions in the blade-to-blade view at the 25% span when the wind speed is at (a) 20 m/s, and (b) 10 m/s

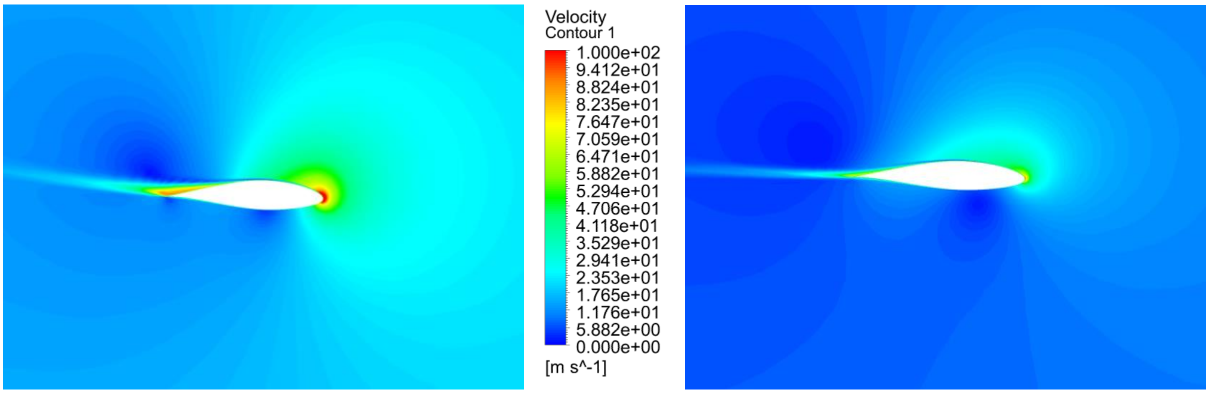

(a) (b)

Figure 11. Velocity distributions in the blade-to-blade view at the 75% span when the wind speed is at (a) 20 m/s, and (b) 10 m/s

Figures 12 and 13 illustrate the pressure contours in the blade-to-blade view for the selected two sections at relatively high and low wind speeds. The pressure is generally the highest near the leading edge where the relative wind velocity interacts with the blade aerofoil. Depending on the speed of the wind, the pressure distributions over the aerofoil surfaces change. At higher wind speeds, the high-pressure concentration is seen on the pressure surface near the leading edge whereas it is slightly shifted towards the leading edge when interacting with low wind speeds. The difference in pressure distribution between the two surfaces is higher at the wind speed of 20 m/s compared to that of 10 m/s. These differences in both velocity and pressure distributions, which are constantly changing in time, impose aerodynamic loads to the blade structure. Figure 14 presents the coefficient of forces, denoted by F/F_{max} and calculated as *(Force on Blade - Average Force on Blade)/(Maximum Force on Blade)*, over the physical time of 0.5 sec obtained from different inflow cases. Due to the nature of the harmonic inflow wakes, loads of the blade are sinusoidal of which the frequencies are similar to that of the inflow wakes whereas the loads are stable in the steady inflow case. The amplitude of the forces distributed over the blade surfaces also depends on the wake frequencies and it gets larger as the frequency increases. Not only the aerodynamic loads could result in the blade structure vibration but also the resonance could occur when the wake frequency is close to the natural frequencies of the blade, which is dangerous for the blade and the wind turbine. Thus, it is also very important to analyse the aeroelasticity of the wind turbine rotor which will be discussed in the next section.

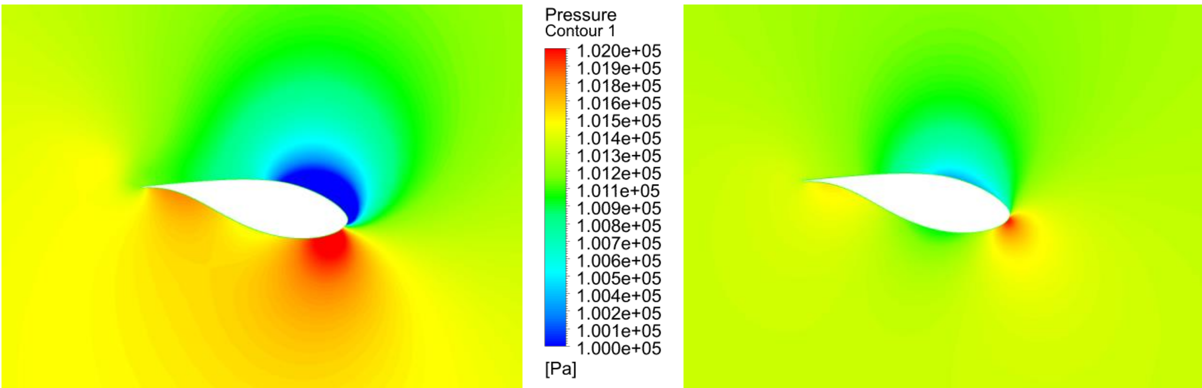

(a) (b)

Figure 12. Pressure distributions in the blade-to-blade view at the 25% span when the wind speed is at (a) 20 m/s, and (b) 10 m/s

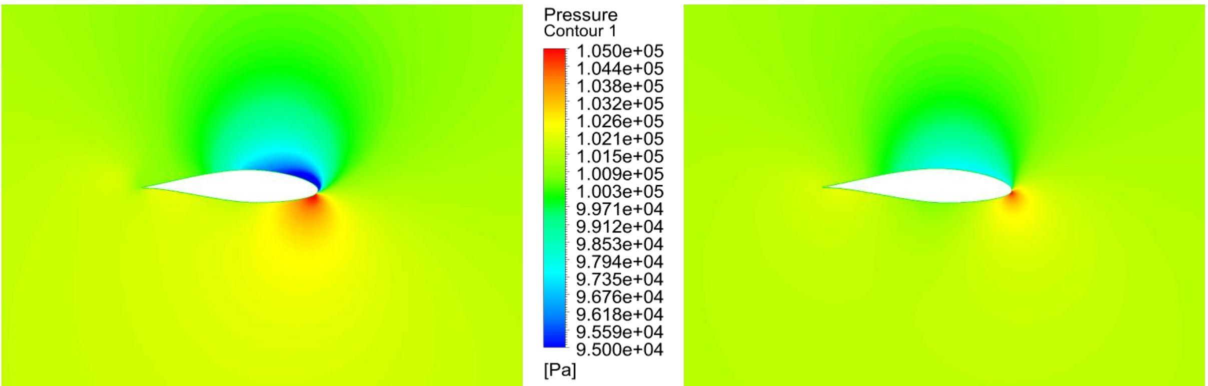

(a) (b)

Figure 13. Pressure distributions in the blade-to-blade view at the 75% span when the wind speed is at (a) 20 m/s, and (b) 10 m/s

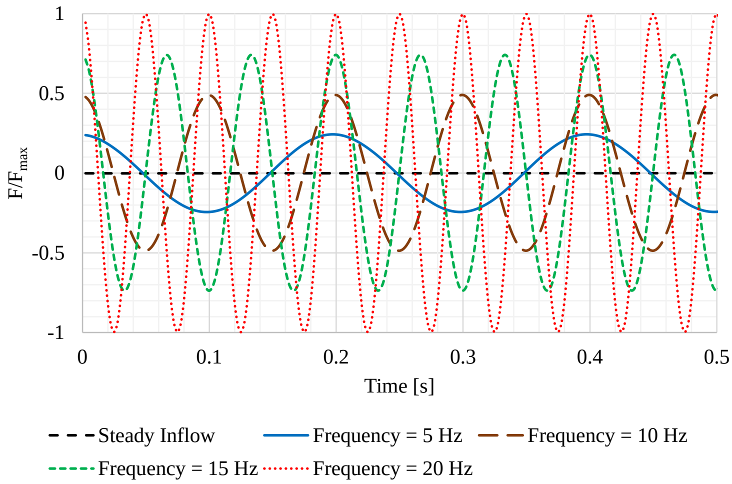

Figure 14. Coefficients of forces distributed over the blade surfaces from the steady inflow case and the harmonic inflow cases

It can be concluded from this analysis that the flow is affected by all wakes considered in this study. The unsteadiness of the inflow wake has a direct impact on the flow field around the rotor imposing aerodynamic loads to the blade structure. Depending on the frequency and the amplitude of the wake, the rate of impact on the aerodynamics of the rotor will vary. Very good agreements between the time domain method and the frequency domain method are obtained in this work which ensures that the frequency domain solution method can be used reliably to analyse the aerodynamics of the wind turbine considering the inflow wakes and unsteadiness. The computation time required by the frequency domain solution method is at least one order of magnitude less than the time domain solution method. The details of the computational cost are presented in Section (4.3).

4.2 Aeromechanical Analysis of the MEXICO-Experiment Wind Turbine

The aeromechanical analysis of the selected wind turbine is discussed in this section. Two different materials, namely an Aluminium Alloy and a composite material, are used with the purpose of analysing the effect of material properties on the aeromechanical performance of the wind turbine blade. It should also be noted that the materials used in this study may not necessarily be the actual material properties used for the wind turbine blades. Before performing the CFD simulations, the natural frequencies and the structural mode shapes of the blade are computed using an FEA method. The first natural frequencies of the blade using an Aluminium Alloy and a composite material, obtained from the modal analysis, are 15.611 Hz and 6.82 Hz, respectively. The frequency domain solution method combined with a phase shift solution method is applied for the aeromechanical analysis of the wind turbine for the considered IBPA value. It is understood that the experimental data for this analysis are not available and thus, the frequency domain solution method is validated against the time domain solution method. For the blade vibration, the first vibration mode is prescribed in which the first natural frequency is defined to be the vibration frequency. In the aeromechanical analysis of turbomachines, relatively small amplitudes are typically used. However, previous studies suggest that the deflection of the blade can be up to 9% of the blade span [30]. Therefore, a relatively large amplitude of 9% of the span is used in this study. The IBPA for this simulation is set to 120 degrees.

The unsteady pressure distributions can be described, similar to previous cases, in terms of the time-averaged pressure and unsteady pressure amplitude coefficients, and they are calculated as shown in Eq. (18). However, in these cases, the sources of flow unsteadiness are associated with blade vibration. The time-averaged pressure and unsteady pressure amplitude coefficients extracted at two blade sections, 30% and 90% span sections, obtained from the time domain solution method and frequency domain solution method, for the selected two materials are compared to each other and shown in Figs. 15-18. The results obtained from the two methods are in good agreement with each other for all cases which indicates that the frequency domain method captures the unsteady flow adequately even when using a relatively large amplitude of vibration. Good agreements are also obtained at other blade sections, but they are not shown in this section to keep it more concise. The unsteady pressure distributions show that some fluctuations are seen at the blade inner region if the composite material is used. Pressure contours are also presented in Fig. 19 for visualization of the pressure distributions over the blade surfaces.

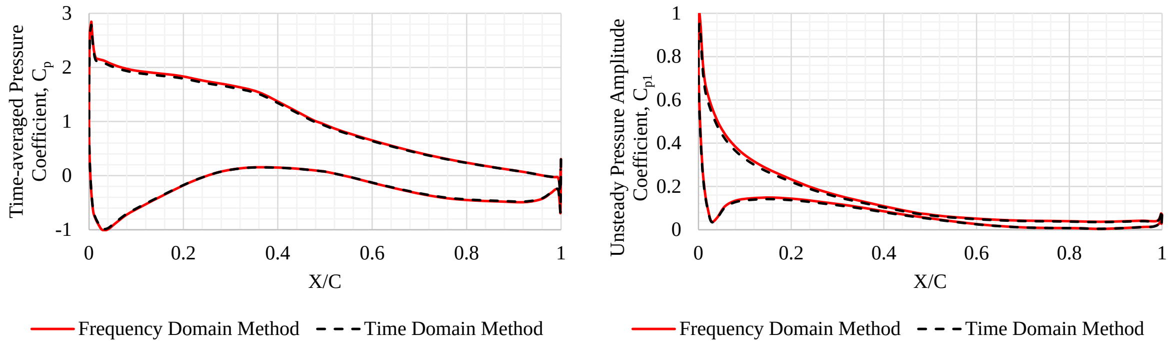

(a) (b)

Figure 15. (a) Time-averaged pressure and (b) unsteady pressure amplitude coefficient distributions over the blade with Aluminium Alloy at the 30% blade span computed from the time domain method *(dotted line)* and the frequency domain method *(line)*

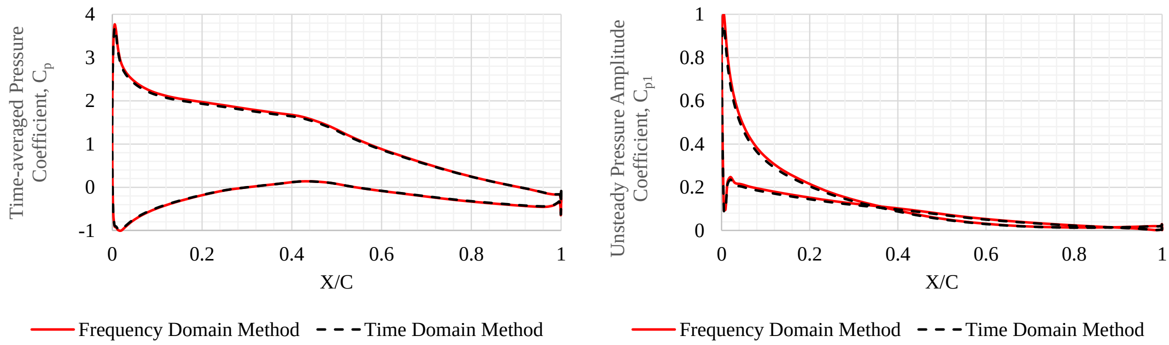

(a) (b)

Figure 16. (a) Time-averaged pressure and (b) unsteady pressure amplitude coefficient distributions over the blade with Aluminium Alloy at the 90% blade span computed from the time domain method *(dotted line)* and the frequency domain method *(line)*

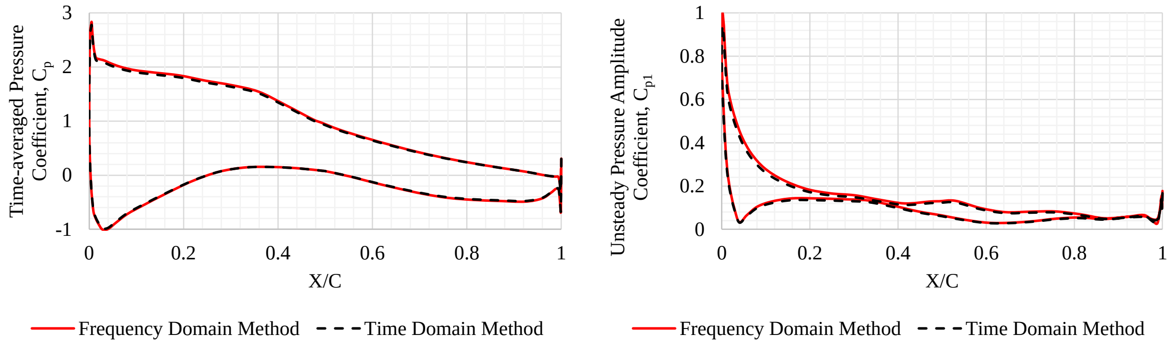

(a) (b)

Figure 17. (a) Time-averaged pressure and (b) unsteady pressure amplitude coefficient distributions over the blade with composite material at the 30% blade span computed from the time domain method *(dotted line)* and the frequency domain method *(line)*

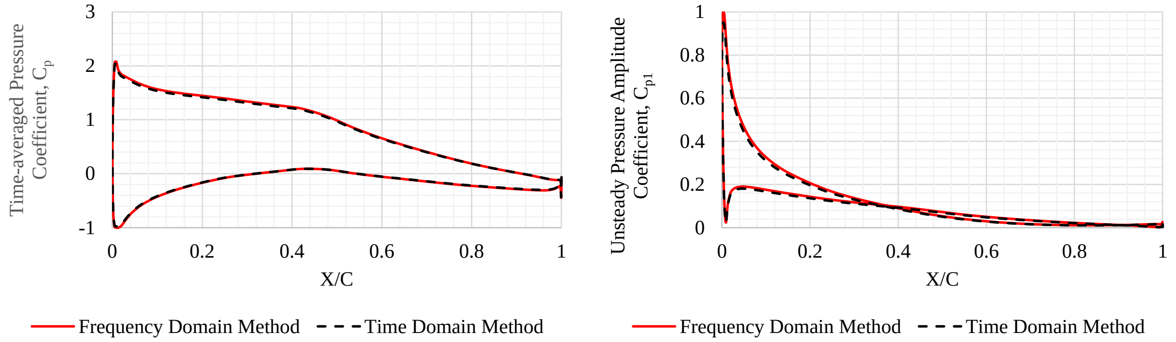

(a) (b)

Figure 18. (a) Time-averaged pressure and (b) unsteady pressure amplitude coefficient distributions over the blade with composite material at the 90% blade span computed from the time domain method *(dotted line)* and the frequency domain method *(line)*

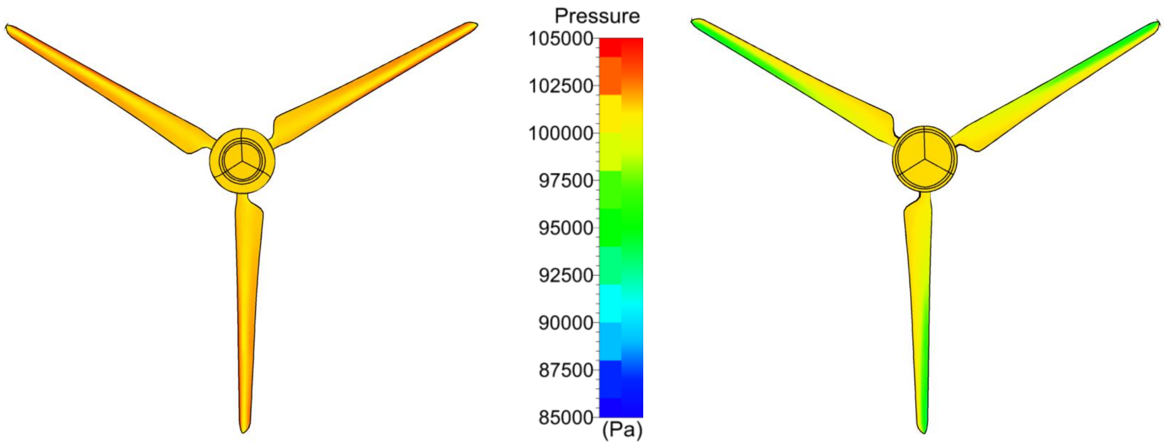

(a) (b)

Figure 19. Pressure contours on (a) pressure surface and (b) suction surface of the MEXICO-Experiment wind turbine rotor blades

Figure 20 presents the coefficient of the forces, expressed as F/F_{max}, applied on the blade surfaces over a complete vibration period due to the blade vibration using two materials. These force coefficients are calculated as *(Force on Blade – Average Force on Blade)/(Maximum Force on Blade)*. As seen, forces applied on the blade is reduced by 6% with the composite material. As the magnitude of forces applied on the blade is directly associated with the structural responses, the composite material can reduce the risk of aeroelastic instability associated with the blade vibrations. Furthermore, as the IBPA of 120 degrees is used in this study, three blades are vibrating out of phase with each other which could potentially impose the instability to the structure even greater. Figure 21 shows the displacement profiles over two vibration periods as well as the displacement contour for visualization of the blade deflection. The blade 1 represents the one at the 12 o'clock position. Positive and negative values of the displacement represent the blade deflecting backwards and forward, respectively.

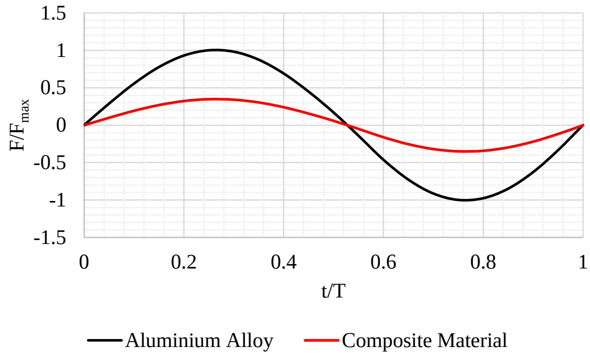

Figure 20. Coefficient of forces applied on the surfaces of the blade using an Aluminium Alloy *(black line)* and a composite material *(red line)* over one vibration period

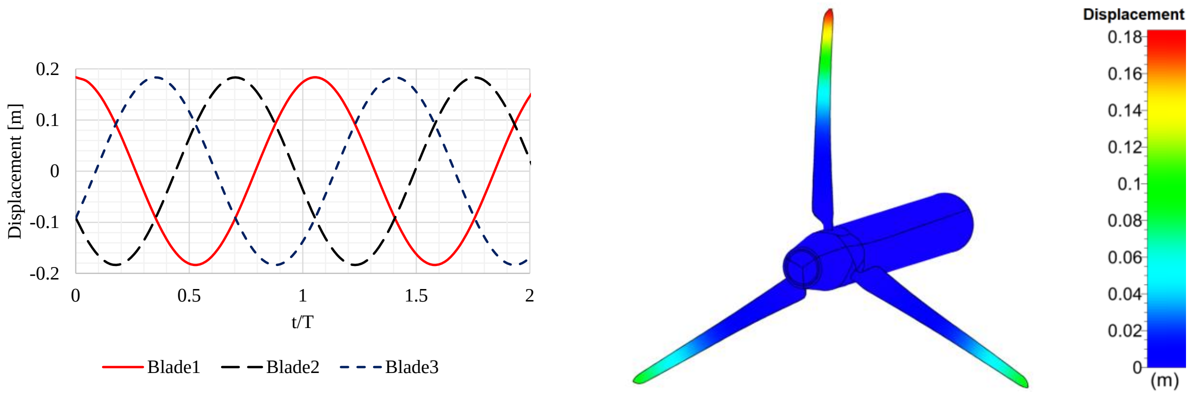

(a) (b)

Figure 21. (a) Displacement profile over two vibration periods and (b) displacement contour of the MEXICO-Experiment wind turbine rotor blades

The aeroelasticity parameter, known as the aerodynamic damping, can be calculated based on the aerodynamic work per vibration cycle and it can be expressed as:

$$W = \int_{t_0}^{t_0+T} \int_A p\vec{v}.\hat{n}dAdt \tag{19}$$

where t_0 is the initial time, T is the vibration period, p is the fluid pressure, v is the velocity of the blade due to the imposed displacement, A is the blade surface area, and $\hat{n}$ is the surface normal unit vector. The aerodynamic damping can be computed as $W/m\omega_v^2 D_{max}^2$ where m is the modal mass, ω_v is the vibration frequency, and D_{max} is the maximum displacement amplitude. If the aerodynamic damping is positive, the blade vibration can be considered stable. The aerodynamic damping values, obtained from the time domain solution method and the frequency domain solution method, for the blade with two materials are outlined in Table 2. As seen, the results obtained are close to each other. The aerodynamic damping values are positive indicating that the vibration is damped in both cases. However, the composite material can provide better stability as the aerodynamic damping is larger than that of Aluminium Alloy. This is also consistent with Fig. 20 in which the forces applied on the blade surfaces are lower with the composite material. Aerodynamic power distributions on both pressure and suction surfaces of the blade can be seen in Fig. 22 which denotes that the blade has the stabilizing effect on both surfaces around the tip of the blade. Overall, it can be concluded that the frequency domain solution method can be reliably used for the aeromechanical analysis of wind turbine rotors and blades considering large deflections with different IBPA values. Only a single passage domain with one blade is required for this analysis with the proposed nonlinear frequency domain solution method.

Table 2. Aerodynamic damping values of the blade with two selected materials

Material	**Time Domain Method**	**Frequency Domain Method**
Aluminium Alloy	0.227	0.230
Composite Material	0.698	0.707

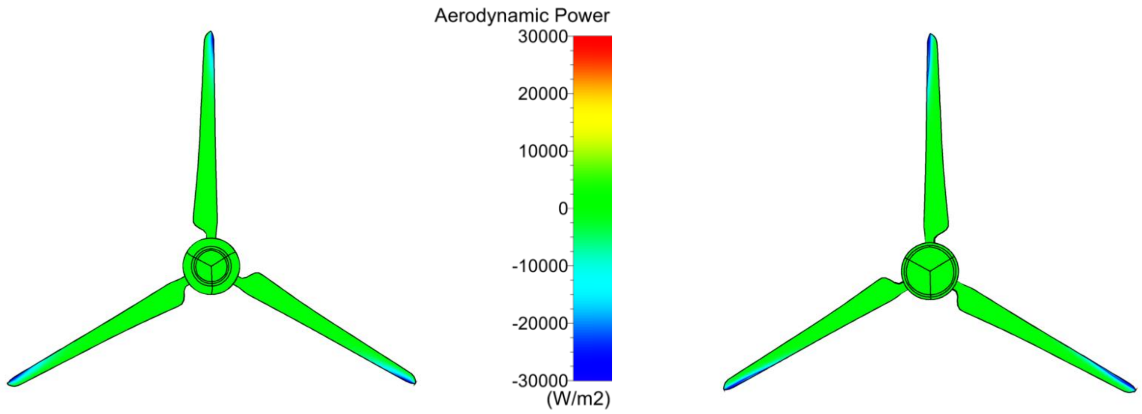

(a) (b)

Figure 22. Aerodynamic power contours on (a) pressure surface and (b) suction surface of the blade

4.3 Computational Costs

All simulations discussed are performed on a single CPU with a 3.40 GHz Intel (R) Core (TM) i5-7500 CPU. With the time domain method, it requires much more CPU time as the full domain with all three blades is used in the simulation whereas only a single passage domain, which is 1/3 of the full domain with a single blade, is required for the frequency domain method. In terms of computation time, it takes 3 hours using the frequency domain method, but it takes about 150 hours if the time domain method is used.

5. CONCLUSIONS

The aerodynamic and aeromechanical analysis of a test case wind turbine are conducted using a highly efficient nonlinear frequency domain solution method in this paper.

First of all, the aerodynamic analysis of the MEXICO-Experiment wind turbine generating the inflow wakes at the inlet is presented. The CFD model used in this work is validated against the experiment as well as the previous simulation, and a good agreement is obtained between them. Using the validated CFD model, the harmonic inflow wakes at different frequencies are generated at the inlet and the effects of the inflow unsteadiness on the aerodynamics of the wind turbine rotor are analysed. The nonlinear frequency domain solution method is employed for this analysis and validated against the conventional time domain method. It is shown that the results obtained from both methods are in a very good agreement. Flow visualisations in terms of velocity and pressure distributions indicate that the flow fields around of the rotor are influenced by the inflow wakes and the unsteadiness of the flow imposes aerodynamic loads to the blade structure. The effects of the inflow wakes on the flow fields are visible at all frequencies whereas the amplitude of forces applied on the blade gets larger with increasing frequencies. Therefore, it can be concluded from this analysis that the unsteadiness of the inflow wakes has an impact on the aerodynamic flow field around the wind turbine rotor, and it could also influence aeroelasticity of the wind turbine significantly as the forces applied on the blade are directly associated with the wake frequencies. The frequency domain method can be used for the aerodynamic analysis of the wind turbine rotor considering the inflow wakes and unsteadiness.

The aeromechanical analysis of the selected wind turbine is then conducted using two different materials. The frequency domain method combining with the phase shift method is used for these computations. Relatively large deflection of 9% of the span is considered in this analysis. The proposed frequency domain solution method is validated against the conventional time domain solution method. The time-averaged and unsteady pressure distributions over the blade surfaces computed using both methods are compared between them, and the results obtained are close to each other. The aerodynamic damping values indicate that the blade vibrations are stable in both cases using two materials. However, it is found that the composite material can provide a greater aerodynamic damping value than the Aluminium Alloy even when the blade is vibrating with a large vibration amplitude.

In terms of computational cost, the proposed nonlinear frequency domain solution method can reduce the computation time by one to two orders of magnitude compared to the conventional time domain solution method. In conclusion, the nonlinear frequency domain solution method can be reliably and efficiently used for the aerodynamic analysis as well as the aeromechanical analysis of wind turbines considering relatively large amplitudes of vibration for any IBPA using a single passage domain that reduces the computation time significantly. Furthermore, as this method enables the computation of rotor-stator interactions of multi-stage configurations, the proposed method will be applied to the simulation of complete wind turbines including the tower as well as the simulation of multiple wind turbines in arrays in the future.

ACKNOWLEDGEMENTS

The authors would like to acknowledge the financial support received from the Engineering Physics and Science Research Council of the UK (EPSRC EP/R010633/1).

REFERENCES

1. Hansen M.H (2007) Aeroelastic Instability Problems for Wind Turbines; Wind Energy; 10: 551–577.

2. Wang Q, Wang J, Chen J, Luo S, Sun J (2015) Aerodynamic shape optimized design for wind turbine blade using new airfoil series; Journal of Mechanical Science and Technology; 29 (7): 2871-2882.

3. Wang L, Liu X, Renevier N, Stables M, Hall G.M (2014) Nonlinear aeroelastic modelling for wind turbine blades based on blade element momentum theory and geometrically exact beam theory; Energy; 76: 487-501.

4. Fernandez G, Usabiag H, Vandepit D (2018) An efficient procedure for the calculation of the stress distribution in a wind turbine blade under aerodynamic loads; Journal of Wind Engineering & Industrial Aerodynamics; 172: 42–54.

5. Rafiee R, Tahani M, Moradi M (2016) Simulation of aeroelastic behavior in a composite wind turbine blade; Journal of Wind Engineering & Industrial Aerodynamics; 15: 60–69.

6. Lee H, Lee D (2019) Numerical investigation of the aerodynamics and wake structures of horizontal axis wind turbines by using nonlinear vortex lattice method; Renewable Energy; 132: 1121-1133.

7. Riziotis V.A, Manolas D.I, Voutsinas S.G (2011) Free-wake Aeroelastic Modelling of Swept Rotor Blades; Conference: EWEA; At Brussels, Belgium.

8. Jeong M.S, Kim S.W, Lee I, Yoo S.J, Park K.C (2013) The impact of yaw error on aeroelastic characteristics of a horizontal axis wind turbine blade; Renewable Energy; 60: 256-268.

9. Rodriguez S.N, Jaworski J.W (2019) Strongly-coupled aeroelastic free-vortex wake framework for floating offshore wind turbine rotors. Part 1: Numerical framework; Renewable Energy; 141: 1127-1145.

10. Rodriguez S.N, Jaworski J.W (2020) Strongly-coupled aeroelastic free-vortex wake framework for floating offshore wind turbine rotors. Part 2: Application; Renewable Energy; 149: 1018-1031.

11. Kaya M.N, Kose F, Ingham D, Ma L, Pourkashanian M (2018) Aerodynamic performance of a horizontal axis wind turbine with forward and backward swept blades; Journal of Wind Engineering & Industrial Aerodynamics; 176: 166–173.

12. Lee H.M, Kwon O.J (2020) Performance improvement of horizontal axis wind turbines by aerodynamic shape optimization including aeroelastic deformation; Renewable Energy; 147: 2128-2140.

13. Liu Y, Xiao Q, Incecik A, Peyrard C, Wan D (2017) Establishing a fully coupled CFD analysis tool for floating offshore wind turbines; Renewable Energy; 112: 280-301.

14. Wang L, Quant R, Kolios A (2016) Fluid structure interaction modelling of horizontal-axis wind turbine blades based on CFD and FEA; Journal of Wind Engineering & Industrial Aerodynamics; 158: 11-25.

15. Dai L, Zhou Q, Zhang Y, Yao S, Kang S, Wang X (2017) Analysis of wind turbine blades aeroelastic performance under yaw conditions; Journal of Wind Engineering & Industrial Aerodynamics; 171: 273–287.

16. Yu D.O, Kwon O.J (2014) Predicting wind turbine blade loads and aeroelastic response using a coupled CFD-CSD method; Renewable Energy; 70: 184-196.

17. Dose B, Rahimi H, Herraez I, Stoevesandt B, Peinke J (2018) Fluid-structure coupled computations of the NREL 5 MW wind turbine by means of CFD; Renewable Energy; 129: 591-605.
18. Dose B, Rahimi H, Stoevesandt B, Peinke J (2020) Fluid-structure coupled investigations of the NREL 5 MW wind turbine for two downwind configurations; Renewable Energy; 146: 1113-1123.

19. Wang L, Liu X, Kolios A (2016) State of the art in the aero-elasticity of wind turbine blades: Aero-elastic modelling; Renewable and Sustainable Energy Review; 64: 195–210.

20. O'Brien J.M, Young T.M, O'Mahoney D.C, Griffin P.C (2017) Horizontal axis wind turbine research: A review of commercial CFD, FE codes and experimental practices; Progress in Aerospace Sciences; 92: 1–24.

21. He L, Ning W (1998) An Efficient Approach for Analysis of Unsteady Viscous Flows in Turbomachines; AIAA J.; 36 (11): 2005–2012.

22. Hall K, Lorence C (1993) Calculation of Three-Dimensional Unsteady Flows in Turbomachinery Using the Linearized Harmonic Euler Equations; ASME J. Turbomach.; 115 (4): 800–809.

23. Hall K, Thomas J, Clark W (2002) Computation of Unsteady Nonlinear Flows in Cascades Using a Harmonic Balance Technique; AIAA J.; 40 (5): 879–886.

24. He L (2008) Harmonic Solution of Unsteady Flow Around Blades With Separation; AIAA J.; 46 (6): 1299–1307.

25. Rahmati M.T, He L, Wells R.G (2010) Interface treatment for harmonic solution in multi-row aeromechanic analysis; Proceedings of ASME Turbo Expo 2010: Power for Land, Sea, and Air; June 14-18, Glasgow, UK.

26. Rahmati M.T, He L, Li Y.S (2012) Multi-row interference effects on blade aeromechanics in compressor and turbine stages; 13th International Symposium on Unsteady Aerodynamics, Aeroacoustics and Aeroelasticity of Turbomachines (ISUAAAT); September 11-14, Tokyo, Japan.

27. Rahmati M.T, He L, Li Y.S (2015) The Blade Profile Orientations Effects on the Aeromechanics of Multirow Turbomachines; J. Eng. Gas Turbines Power; 138 (6): 062606.

28. Rahmati M.T, He L, Wang D.X, Li Y.S, Wells R.G, Krishnababu S.K (2014) Nonlinear Time and Frequency Domain Method for Multi-Row Aeromechanical Analysis; ASME J. Turbomach.; 136 (4): 041010.

29. Horcas S.G, Debrabandere F, Tartinville B, Hirsch C, Coussement G (2017) Rotor-tower interactions of DTU 10MW reference wind turbine with a non-linear harmonic method; Wind Energy; 20: 619–636.

30. Horcas S.G, Debrabandere F, Tartinville B, Hirsch C, Coussement G (2017) Extension of the Non-Linear Harmonic method for the study of the dynamic aeroelasticity of horizontal axis wind turbines; Journal of Fluids and Structures; 73: 100–124.

31. Howison J, Thomas J, Ekici K (2018) Aeroelastic analysis of a wind turbine blade using the harmonic balance method; Wind Energy; 21: 226–241.

32. Drofelnik J, Ronch A.D, Campobasso M.S (2018) Harmonic balance Navier-Stokes aerodynamic analysis of horizontal axis wind turbines in yawed wind; Wind Energy; 21: 515–530.

33. Win Naung S, Rahmati M.T, Farokhi H (2019) Aerodynamic Analysis of a Wind Turbine with Elevated Inflow Turbulence and Wake using Harmonic Method; Proceedings of the ASME 2019 38th International Conference on Ocean, Offshore and Arctic Engineering (OMAE2019); June 9-14, Glasgow, Scotland.

34. Win Naung S, Rahmati M.T, Farokhi H (2019) Aeromechanical Analysis of Wind Turbines using Non-linear Harmonic Method; Proceedings of the ASME 2019 38th International Conference on Ocean, Offshore and Arctic Engineering (OMAE2019); June 9-14, Glasgow, Scotland.

35. Schepers J.G, Pascal L, Snel H (2010) First results from Mexnext: Analysis of detailed aerodynamic measurements on a 4.5 m diameter rotor placed in the large German Dutch Wind Tunnel DNW; The European Wind Energy Conference and Exhibition (EWEC); April 20-23, Warsaw, Poland.

36. Schepers J.G, Boorsma K, Munduate X (2012) Final Results from Mexnext-I: Analysis of detailed aerodynamic measurements on a 4.5 m diameter rotor placed in the large German Dutch Wind Tunnel DNW; The Science of making Torque; October 9-11, Oldenburg, Germany.

37. Schepers J.G, Snel H (2007) Model Experiments in Controlled Conditions, Final report; ECN-E-07-042, ECN.

38. Schepers J.G, Boorsma K, Kim C, Cho T (2012) Final report of IEA Task 29, Mexnext (Phase 1): Analysis of Mexico wind tunnel Measurements; ECN-E–12-004, ECN.

39. Carrion M, Woodgate M, Steijl R, Barakos G (2014) CFD and Aeroelastic Analysis of the MEXICO Wind Turbine; Journal of Physics. Conf. Ser.; 555 012006.

40. Bechmann A, Sørensen N.N, Zahle F (2011) CFD simulations of the MEXICO rotor; Wind Energy; 14: 677–689.

41. Sørensen N.N, Zahle F, Boorsma K, Schepers G (2016) CFD computations of the second round of MEXICO rotor measurements; Journal of Physics. Conf. Ser.; 753 022054.

42. Herraez I, Medjroubi W, Stoevesandt B, Peinke J (2014) Aerodynamic Simulation of the MEXICO Rotor; Journal of Physics. Conf. Ser.; 555 012051.

43. Plaza B, Bardera R, Visiedo S (2015) Comparison of BEM and CFD results for MEXICO rotor aerodynamics; Journal of Wind Engineering & Industrial Aerodynamics; 145: 115–122.

44. He J, Fu Z.F (2001) Modal Analysis; Butterworth-Heinemann; ISBN 978-0-7506-5079-3.

45. Rao S.S (2011) Mechanical Vibrations; Pearson; ISBN 978-0-13-212819-3.